TRI PP 94 104
Dec 1994

The CHAOS Spectrometer for Pion Physics at TRIUMF

G.R. Smith[a], P.A. Amaudruz[a], J.T. Brack[a*], L. Felawka[a], A. Gorelov[a†], R.A. Henderson[a], D.F. Ottewell[a], P. Vincent[a], Y. Wu[a‡], F. Bonutti[b], P. Camerini[b], N. Grion[b], R. Rui[b], J. Hoey[c], G. Hofman[c], M. Kermani[c], D. Maas[c], S. McFarland[c], K. Raywood[c], M.E. Sevior[c§], E.L. Mathie[d], R. Tacik[d], P. Reeve[e], R.A. Ristinen[f], E.F. Gibson[g], R. Meier[h¶], H.M. Staudenmaier[h]

[a] *TRIUMF, Vancouver, B.C., Canada V6T 2A3*
[b] *Instituto Nazionale di Fisica Nucleare, Sezione di Trieste, and Dipartimento di Fisica dell'Università di Trieste, 34127 Trieste, Italy*
[c] *Physics Dept., University of British Columbia, Vancouver, B.C., Canada V6T 2A6*
[d] *University of Regina, Regina, Saskatchewan, Canada, S4S 0A2*
[e] *University of Victoria, Victoria, B.C., Canada, V8W 2Y2*
[f] *University of Colorado, Boulder, CO 80309, USA*
[g] *California State University, Sacramento CA 95819, USA*
[h] *Universität Karlsruhe, D-7500 Karlsruhe, Germany*

Abstract

The Canadian high acceptance orbit spectrometer (CHAOS) is a unique magnetic spectrometer system recently commissioned for studies of pion induced reactions at TRIUMF. It is based on a cylindrical dipole magnet producing vertical magnetic fields up to 1.6 T. The scattering target is located in the center of the magnet. Charged particle tracks produced by pion interactions there are identified using four concentric cylindrical wire chambers surrounding the target. Particle identification and track multiplicity are determined by cylindrical layers of scintillation counters and lead-glass Čerenkov counters, which also provide a first level trigger. A sophisticated second level trigger system permits pion fluxes in excess of 5 MHz to be employed. The detector subtends 360° in the horizontal plane, and ±7° out of this plane for a solid angle coverage approximately 10% of 4π sr. The momentum resolution delivered by the detector system is 1% (σ).

(submitted to Nucl. Instrum. Methods)

*Present address: University of Colorado, Boulder, CO 80309, USA.
†Present address: Simon Fraser University, Vancouver, B.C., Canada.
‡Present address: Institute of Atomic Energy, Beijing, China.
§Present address: University of Melbourne, Parkville, Vic., 3052 Australia.
¶Present address: TRIUMF, Vancouver, B.C. Canada V6T 2A3.

1. Introduction

The Canadian high acceptance orbit spectrometer (CHAOS) is a magnetic spectrometer with an angular acceptance of a full 360° in the horizontal plane, intended for studies of pion-induced reactions at TRIUMF. With this device, data are acquired simultaneously at every scattering angle within ±7° of the horizontal plane. The coincidence efficiency for reactions leading to two body final states is close to unity. The momentum resolution (dp/p) of CHAOS is ~1% (σ).

This unique facility can address a number of interesting 'second generation' experiments with pion beams. The complete angular acceptance makes it particularly well suited for coincidence measurements. However, it is also meant to address singles experiments involving low cross sections. Each of these areas has proven difficult to study until now due to the exorbitant amount of beam time required for angle-by-angle measurements with conventional spectrometers.

The initial CHAOS physics program has focused on a systematic investigation of the $H(\pi^{\pm},2\pi)$ reaction in a series of exclusive measurements. For incident π^-, the $H(\pi^-,\pi^+\pi^-)n$ and the $H(\pi^-,\pi^-\pi^0)p$ channels were measured simultaneously by detecting the two charged particles in the final state in coincidence. Likewise for incident π^+, the $H(\pi^+,\pi^+\pi^+)n$ and the $H(\pi^+,\pi^+\pi^0)p$ channels were measured simultaneously. Pion bombarding energies of 220, 240, 260, 280, and 300 MeV were studied and approximately 10,000 $(\pi,2\pi)$ events were recorded at each energy for the channels with two charged pions in the final state. By measuring both reaction channels for both incoming pion polarities from near threshold up to $T_\pi = 300$ MeV over a broad angular range, it is possible to isolate the contributions from the various diagrams contributing to this process [1]. One goal of these measurements is to improve the values for the S-wave isospin 0 and 2 $\pi\pi$ scattering lengths a_0^0 and a_2^0, which are predicted [2] within the framework of chiral perturbation theory to have values of 0.20 ± 0.01 and -0.042 ± 0.002, respectively. In addition, these data should permit the extraction of $\pi\pi$ scattering amplitudes as a function of energy.

Another of the physics goals in the CHAOS arena is the study of the $\pi^{\pm}\vec{p}$ analyzing power A_y between 20 and 140 MeV, and between 45° and 180° . No data have ever been published below 98 MeV. This information is crucial for phase shift analyses of πN scattering. Near pion bombarding energies of 50 MeV there exists a strong S-P interference for backward angle π^-p scattering, and strong Coulomb-nuclear interference at forward angles for π^+p scattering, which will be exploited in these studies. The analyzing power, itself an interference of amplitudes, is especially sensitive to the values of the smaller partial waves which are only poorly determined from measurements of the differential cross section alone. The CHAOS A_y results will be used to distinguish between conflicting measurements of the differential cross section at low energies. The poor agreement between previous differential cross section measurements has made it virtually impossible to produce reliable πN phase shifts. The CHAOS analyzing power data will also provide independent constraints on the value of the πN Σ term [3], which is an explicit measure of chiral symmetry breaking. The πN Σ term, in turn, can be related to the strange quark content of the proton. This experiment, as well as the $(\pi,2\pi)$ program, tests predictions of chiral perturbation theory [4], the low energy approximation of quantum chromodynamics (QCD).

2. Detector Overview

The experimental challenges posed by the $\pi^{\pm}\vec{p}$ and $(\pi,2\pi)$ measurements are similar in that they both require coincident particle detection with moderate (~1%)

momentum resolution, and they both are characterized by cross sections which drop below the 10 μb/sr level in conjunction with background processes often several orders of magnitude larger. Furthermore, systematic measurements covering a broad range in angle and energy are needed. As a result a detector ensemble was designed [5] which could address these challenges. Other factors in the design include the following: The momentum resolution of the spectrometer should match that delivered by the beamline. The TRIUMF beamlines deliver approximately 5% dp/p, which can be reduced by closing slits at the intermediate focus at the expense of pion flux. In order to achieve even the modest goal of 1% in momentum resolution, considerable care must be devoted to a design which minimizes multiple scattering of the outgoing tracks. At the same time, however, full angular coverage was deemed an essential feature, and to facilitate acceptance calculations for the experiments, it was decided to construct self-supporting wire chambers which contained no support posts or other features which would otherwise produce shadows in the acceptance. In order to remove potential ambiguities in track sorting and to provide some level of redundancy, at least 5 hits per track were desired (the final design provides up to 11 hits per track). The trigger system must permit the full intensity of the available beam to be utilized (~5 MHz), which implies use of a sophisticated multi-level hardware trigger system. The detector must accommodate polarized, cryogenic, and solid targets. Good momentum resolution is required for all scattering angles. Good particle identification, in particular π/p/e, is essential. Finally, a large cylindrical dipole magnet was available, the use of which resulted in a considerable savings in the total cost of the project.

In order to achieve good momentum resolution for all scattering angles, the traditional approach of orienting the magnetic field axis of the spectrometer longitudinal to the incident beam was abandoned in favor of an orientation in which the magnetic field axis is normal (vertical) to the nominal (horizontal) scattering plane. The scattering target is then situated in the center of the cylindrical dipole magnet, and surrounded by concentric, cylindrical wire chambers to record the spatial coordinates of charged particle tracks emanating from the target. Three wire chambers are located in a region of uniform magnetic field, where the trajectory of charged particles is circular. A fourth chamber consisting of eight (cylindrical) planes is placed outside the region of uniform magnetic field to improve the momentum resolution of the device and to provide the extra redundancies needed for unambiguous track sorting.

The GEANT Monte Carlo code was used to optimize the radii chosen for the wire chambers, to choose the number of chambers and wire planes required, to find the spatial resolution required of the wire chambers, and to help determine what materials were best suited for their construction. The most crucial parameter in these studies was, of course, the overall momentum resolution. However, this was considered in the context of the philosophy that the chambers would have to be self-supporting with no support structures which would introduce angle-dependent corrections to the spectrometer solid angle.

The facility which emerged from these design considerations [6] is a charged particle magnetic spectrometer consisting of a dipole magnet with cylindrical poles 95 cm in diameter and a 20 cm gap. The magnet is capable of producing vertical magnetic fields in excess of 1.6 T. The scattering target is located in the center of the magnet between the poles. An open bore along the central (vertical) axis of the magnet allows insertion of polarized and cryogenic targets. Four concentric cylindrical wire chambers view tracks emanating from the target over a full 360° range in the horizontal plane, with a vertical acceptance of $\pm 7°$. The chambers are enclosed by concentric rings of counter telescopes consisting of two layers of thin plastic scintillators plus Čerenkov detectors. The total solid angle of the facility is ~10% of 4π sr. A

sketch showing the general layout of CHAOS is shown in fig. 1. The four concentric cylindrical wire chambers are denoted WC1-4, with the innermost labelled WC1. The scintillator and Čerenkov blocks which enclose WC4 are shown together with their light guides and photomultiplier tubes (PMTs), and are denoted collectively as the CHAOS fast trigger (CFT) counters. Further details of the detector are shown in fig. 2, which is a zoom of the central region with some sections of the detector cut away for clarity.

3. The Magnet

One of the design features of CHAOS is the ability of the spectrometer to simultaneously measure complete angular distributions and complete angular correlations for two body reactions. In order to meet this criterion, a cylindrical dipole magnet with an exceptionally open geometry (ideally 360° angular acceptance) must be chosen. The magnet must be able to produce a vertical magnetic field which is uniform to ~1% at least over the region between the inner three wire chambers. The magnet must be physically large (r~1 m) in order to accommodate wire chambers, and also capable of producing a large enough field for reasonable (~1%) momentum determination. The $\int$ Bdl of the magnet should be in excess of 1 T-m. The vertical gap must be large enough ($\geq$20 cm) to accommodate the wire chambers and calorimetry. There should be an open bore through the central axis of the magnet large enough ($\geq$12 cm ϕ) to accommodate cryogenic and polarized targets. There should be no yoke or obstruction which might block the acceptance of the device inside a central region two meters in diameter. Finally, the return yoke outside this central region must allow for unobstructed passage of the incident and outgoing beam over a wide range of deflection angles.

An existing magnet at TRIUMF met most of these conditions to a reasonable degree. It is a cylindrical dipole magnet (not superconducting) with an iron return path. It has a 12 cm diameter open bore. Although most conventional magnets have vertical yokes enclosing two sides of the magnet, the CHAOS magnet has narrow vertical return yokes located in each of the four corners of the (roughly square) top and bottom yokes. It has a 95 cm diameter pole. The magnet has been operated at fields in excess of 1.6 T.

The magnet was studied with a variety of computer codes (MAGDES, POISSON, TOSCA). Tapered iron pole tips were added to the existing magnet poles to reduce the gap in the central region to 20 cm. This permits higher maximum magnetic fields than otherwise possible, and also has the effect of flattening the field profile in the region between the pole tips. By adding pole tips to the existing poles instead of reducing the overall gap, the large gap between the coils was kept outside the central region, which greatly facilitates cable access and detector instrumentation. In addition, ring-shaped shims were added to the inner and outer diameters of the pole tips to tailor the field in the central region. Finally, the amount of steel in the upper and lower yokes as well as in the four corner return yokes was doubled to reduce saturation. The four corner yokes were moved to greater radii and reconfigured in order to maximize the open space between the corner yokes and strengthen the support provided between the upper and lower yokes.

Fig. 3 shows the final magnet configuration. The field is uniform to better than 1% between about 5 and 35 cm. The magnet is 1066 mm high and 2235 mm wide, outside dimensions. The B-I curve of the magnet is linear up to about 0.9 T (200 amps) and is already entering saturation at 1.4 T (400 amps).

Extensive two dimensional magnetic field maps were measured at four elevations and four magnetic field settings using a three dimensional Hall probe. The Hall probe

readings were cross checked with an NMR probe in the flat field region. One quadrant of the magnet was mapped in this procedure out to a radius of 1.8 m. No appreciable asymmetry was found in the measured field distribution in the region where the wire chambers are located. These maps are used in the momentum reconstruction routines employed in the analysis of CHAOS events by interpolating the position and central field strength between the points measured in these field maps. An NMR probe situated on the face of the lower pole tip at an approximate radius of 22 cm is used for normalization.

Since the incident pion beam deflects as it traverses the spectrometer, the magnet must be translated perpendicular to the nominal beamline in order to insure that the beam strikes the target. In addition, it is convenient to rotate the spectrometer about its central axis to facilitate the beam entry and exit locations relative to the four corner return yokes. As a result, a stand was built which employs a hydraulic cylinder and four Hillman roller bearing assemblies which ride on a pair of 3.66 m long rails consisting of 2.5 cm x 10.2 cm flat bar grouted (2.5 cm high) onto the floor of the experimental area. This system can translate the entire ~55 ton spectrometer up to 1.8 m from the beamline. In addition a cylindrical crane bearing is also installed which allows the entire spectrometer to be rotated by an AC motor. Shaft encoders are employed in conjunction with digital readout systems designed and built at TRIUMF to read out the translation of the spectrometer to within 0.013 mm and the angle of rotation to approximately 0.0015°. Typical values of the required translation and resulting rotation of the incoming beam at the central target for an incident beam momentum of 300 MeV/c and spectrometer field of 1.0 T are 166.8 mm and 31.8°.

A platform is attached to the magnet on three sides flush with the top surface of the magnet, about 2.5 m off the ground. It provides access to both sides of the six electronics racks situated on top of the magnet, which contain virtually all of the readout electronics for the detector. Personnel access to the electronics platform is possible while the magnet is in the experimental area receiving beam. In order to gain access to the wire chambers for installation, cabling, and repair work, the upper half of the magnet must be removed. Access to the wire chambers is then provided by means of a cart rolling on a horizontal ladder which can be attached to the magnet approximately 20 cm above the top of the wire chambers.

4. Proportional Chambers WC1 and WC2

Factors in the design of the two innermost CHAOS wire chambers include the following: Since these chambers are located near the focus of the incident beam and have small diameters, the rate per wire can be high (roughly 1 MHz per wire for a 2 mm anode pitch). In order to facilitate vertex reconstruction and scattering angle determination, it was deemed necessary to be able to track the incoming pion beam at rates up to 5 MHz with these two chambers, as well as any outgoing tracks. Since WC1 and WC2 are situated in the homogeneous region of the spectrometer magnetic field, the spatial coordinate each delivers can be used in conjunction with the known incoming beam momentum to fully reconstruct the trajectory of the incoming beam onto the target. Vertical tracking (in the direction parallel to the spectrometer field) was also required of these chambers for the same reasons. Monte Carlo calculations indicated that the innermost chamber should be situated at as small a radius as possible and have an angular resolution better than 1/2°. Practical considerations were that some volume had to be left free to accommodate the central target and that it is difficult to construct a cylindrical chamber with an anode pitch less than about 1 mm. The geometry of WC1 was therefore fixed by the dual requirements of 1 mm anode pitch and 1/2° angular resolution. Monte Carlo calculations indicated WC3 was best situated at the outer edge of the uniform field distribution, and that

the optimal radius of WC2 was about halfway between WC1 and WC3. With this radial constraint as well as the 1/2° angular resolution required, a 2 mm anode pitch was chosen for WC2.

The two innermost CHAOS wire chambers are proportional chambers located at radii of 114.59 (WC1) and 229.18 mm (WC2). Each has a half-gap (anode wire to cathode plane distance) of 2 mm, and contains a total of 720 gold-plated tungsten anode wires 12 μm in diameter. The wires cover the entire 360° angular acceptance of the spectrometer with an active height of 70 mm.

Each anode in each chamber is equipped with a preamplifier mounted directly on the chamber. The bipolar Fujitsu MB43458PF quad preamplifier chip was chosen due to its excellent performance and compact size. The 16-channel preamplifier boards also capacitatively decouple the anode high voltage at the input of the preamplifier. Coaxial cables (Alpha 9374) 3 m in length deliver the anode pulses to LeCroy 2735PC amplifier discriminator cards powered in specially constructed crates, each of which contains up to 21 cards. Two such crates are attached to each of the four corner return yokes of the magnet. The ECL outputs of the amplifier/discriminator channels are then delivered on 17 channel flat twisted pair cables (Belden 9V28034) to LeCroy 2731A delay/latch modules which form part of the LeCroy PCOS III readout system. This, as well as all other readout systems associated with the spectrometer, is located on top of the magnet so that the entire spectrometer can be moved from one experimental area to another without disconnecting a single wire upstream of the readout systems. PCOS III was chosen because it provides zero-suppression, programmable delay for each channel relative to the common strobe, and a programmable threshold for each 2735PC card. The system is operated in 'cluster mode', which delivers the centroid (and width) of a cluster of up to 16 adjacent wires including a 'half-wire' bit if the cluster width is even. The spectrometer magnet deflects the tracks passing through WC1 and WC2 sufficiently that several adjacent anodes usually fire for each track, effectively improving the angular resolution of these two chambers by a factor of two, to 1/4°, in the cluster mode of operation. In addition, the LeCroy 2738 PCOS III controllers provide ECL output which is convenient input to the CHAOS second level trigger.

Each of the first two chambers is also equipped with cathode strips inclined 30° with respect to the anode wires, on the outer cathode surface of each chamber. The pitch of these strips is 2 mm (WC1) and 4 mm (WC2). Each of the 360 strips in each chamber is preamplified at the chamber and delivered to 16 channel inverter/amplifier cards via coaxial cables 3 m long. The inverter/amplifier cards were designed and built at TRIUMF and are based on SL560 chips. One crate capable of housing 21 such cards is located on each of the four corner return yokes of the spectrometer magnet. The analog output of these cards is delayed 210 ns by means of RG174/U coaxial cables 40 m long. The delay cables are jacketed in bundles of 16, spooled in pairs and hung on rods fixed to the spectrometer magnet. The delayed cathode signals are digitized in LeCroy 1882F FASTBUS analog to digital converters (ADCs) which are gated by a signal 100 ns wide. The delay is necessary to allow the gate signal to be formed, which is the result of the first level trigger decision based on the number of tracks found in the scintillation counter arrays. The FASTBUS crate is read out with a LeCroy 1821 segment manager/interface which is programmed to perform pedestal subtraction, threshold comparison, and zero suppression. Typically several adjacent cathode strips which are associated with a given cluster of struck anodes survive this procedure. The charge-weighted centroid of the strips is determined, and together with the anode information, the vertical coordinate of the trajectory can be determined in both WC1 and WC2 for tracks separated by more than 30°. The vertical resolution delivered by WC1 (WC2) is 2.4 mm (0.7 mm), as determined in an iterative calibration procedure with non-scattered tracks, and including information

from WC4, discussed below.

The two proportional chambers are of identical construction except for the different radii, anode and cathode pitches. A side section view of WC1 and WC2, including the other detector elements as well, is shown in fig. 4. Each chamber is composed of two independent cylinders. Each cylinder consists of an upper and a lower G10 ring held 70 mm apart by a 1 mm–thick cylinder of rohacell. Rohacell was chosen for its exceptional strength and small density of 50 mg/cm^3, which minimizes multiple scattering. The main drawback of this material is the fact that it contracts as the humidity is lowered, as happens when it is in contact with chamber gas. This effect was kept under control by baking 4 mm–thick sheets of rohacell at 160° C prior to machining to the required size and thickness, as well as gluing stretched foils to the inner and outer surfaces of the rohacell cylinders. The inner cylinder has a 12 μm–thick kapton foil glued to its inner surface, and a 25 μm–thick foil of aluminized mylar glued to its outer surface. The latter serves as the inner cathode plane for the chamber. This plane is in addition covered with a thin layer of graphite to retard polymerization. The anode wires are soldered under 10 g of tension directly to circuit board strips glued to the G10 rings of the inner cylinder, 2 mm from the cathode foil. The cathode strips were photochemically etched on an electro–coated copper/nickel (ECN) foil consisting of 25 μm kapton, 1200 Å copper, and 300 Å nickel which was glued to the inner surface of the outer cylinder. Contact to the strips was achieved using gold–plated spring clips which were in mechanical contact with the strips on one end and soldered to a circuit board on the other. A 12 μm kapton foil was glued to the outer surface of the outer cylinder.

In addition, 25 μm aluminized mylar foils were glued to the G10 rings at ±8 mm from the anode radius in order to isolate the chamber anodes better from outside electromagnetic interference, as well as to provide a nitrogen flushing volume to isolate the chamber gas better from the environment between chambers. Until now that environment has consisted of air. However, the G10 rings were designed to permit foils to be stretched between the rings of adjacent chambers to form a helium bag.

The two independent cylinders of each chamber are joined together by means of natural rubber tubes inserted in the 2.8 mm gap between the inner and outer G10 rings. One such tube is positioned between the top pair of rings, another between the lower pair. The tube is easily positioned by collapsing it into a flat ribbon using a syringe to deflate the tube. Likewise the tube is reinflated with a syringe, forming a gas tight seal and freezing the relative position of the two cylinders. Three 0.7 mm–diameter pins are used to index the two cylinders so that their relative positions can be reproduced after the cylinders are separated during a repair procedure. Repairs are greatly facilitated by having the anode wires on the inner cylinder and the cathode strips on the outer cylinder since once the cylinders are separated, access to either the anodes or cathode strips is unrestricted. Ring stands were built which employ an eccentric system which permits each chamber to be independently rotated and centered with respect to the center of the magnet.

The operating (anode) voltages of WC1 and WC2 are +2500 volts and +2100 volts, respectively. At these voltages, WC1 (WC2) has an anode efficiency of 96% (92%) for minimum ionizing pions. This positive high voltage is daisy–chained to the anodes of each chamber via small printed circuit boards attached to the bottom of the chambers.

WC1 and WC2 operate with a mixture of CF_4 and isobutane gas in an 80:20 ratio. The gas volumes of WC1 and WC2 are 0.2 and 0.4 liters, respectively, and the flow rate of gas through each chamber is approximately 100 cm^3/minute. The CF_4 is recirculated in a closed system built by the TRIUMF detector group [7]. Isobutane detectors are installed in the experimental area as well as in the detector itself to reveal leaks. A further safety measure is a blower located below the magnet which

establishes an air flow from the center of the spectrometer to the outside world, cooling the electronics in the central region and removing any potential isobutane gas pocket at the same time.

Clean spectra from these chambers were acquired only after considerable work was done to eliminate initial noise problems. The most significant improvement was the addition of a copper ground skirt which was soldered directly to the ground plane of the circuit boards to which the anodes were soldered, on the bottom of the chambers. Furthermore, oscillations develop in the 2735 amplifier/discriminator cards unless all inputs and outputs are properly terminated. Discriminator thresholds on the 2735PC cards are set at the maximum value which can be obtained from the PCOS system. Further details on these two chambers are described elsewhere [8].

5. The High Field Drift Chamber WC3

Monte Carlo calculations indicated that the spatial resolution required in WC3 had to be $\leq$ 200 μm (σ) in the scattering plane, and that the radius of this chamber had to be near the outer edge of the flat field region in order to meet the design goal of 1% momentum resolution for the spectrometer. A third chamber inside the flat field region was also desired in order to have an analytic solution for the track momenta. A fast proportional chamber would have been ideal, but even with a 1 mm pitch, it would only deliver an r.m.s spatial resolution of 300 μm. Furthermore, instrumenting a 1 mm pitch chamber at this radius with readout electronics would be prohibitively expensive. In order to keep the cost of WC3 comparable to that associated with each of the other chambers in the spectrometer, and to obtain spatial resolution below 200 μm, it was therefore decided to build a drift chamber.

This option comes with its own set of problems. The design calculations called for a fourth chamber and so multiple scattering in the third chamber had to be minimized. This could only be accomplished in a single (cylindrical) plane drift chamber. Furthermore, the angle at which tracks pass through the chamber can vary by about 90° (±45°), depending on the spectrometer field and track momentum and polarity. Since the spectrometer field can be as large as 1.6 T, the Lorentz angle associated with electrons drifting towards the anodes in WC3 can exceed 90° .

There is a left/right (L/R) ambiguity associated with whether the electrons drifted to the anode from the left or from the right of the anode. A measure of the drift time alone does nothing to resolve this ambiguity. The effects of large magnetic fields and varying incident track angle combine to such a degree in CHAOS that traditional solutions to the L/R ambiguity no longer work. Usually, the charge induced on cathode wires adjacent to the anode or on cathode strips located to the left and right of the anode is used to resolve the ambiguity. Since in the CHAOS environment (high B field, low E field, and varying incident track angle) the anode avalanche can occur in front of or behind the anode instead of to the left or to the right, these techniques fail. A simple yet novel technique was therefore applied by instrumenting both the inner and outer (cylindrical) cathode planes with cathode strips. Each drift cell contains four cathode strips, two on the inner plane, two on the outer plane, centered on the anode. Instead of examining the difference in charge induced on adjacent strips, the diagonal combination is taken, which permits the L/R ambiguity to be resolved for all track angles and magnetic fields up to 1.6 T. This technique was studied in detail with five prototype chambers, and the results are published in ref. [9].

The WC3 anodes are located at a radius of 343.78 mm, just inside the tapered pole tips of the spectrometer magnet. The chamber consists of alternating anode and cathode wires in an approximately rectangular cell geometry. The anode pitch is 15 mm (2.5°), and the half gap of the chamber is 3.75 mm. Therefore the maximum

drift distance is nominally 7.5 mm (approximately 150 ns maximum drift time at zero magnetic field). As mentioned above, each of the 144 cells in the chamber is equipped with four cathode readout strips. In addition, two smaller strips are implemented in the corners of each cell to improve the electric field in those regions. The cell geometry is shown in fig. 5.

The anode signals are capacitatively decoupled from the high voltage and preamplified at the chamber, and brought out of the detector on ten foot coaxial cables to LeCroy 2735DC amplifier discriminator cards positioned in crates on the four corners of the magnet, as with WC1 and WC2. The 2735DC output is carried on ECL ribbon cables to the PCOS III system as with the two inner chambers. However, the WC3 ECL cables are not terminated at the 2731A PCOS input, but continue to the input of LeCroy 4291 time-to-digital converters (TDCs), so that each anode of WC3 is read out by the PCOS III system as well as the 4290 TDC system. The WC3 PCOS readout is used in conjunction with that from WC1 and WC2 to form the input to the second level trigger. The 4290 readout is used to digitize the drift times and take the WC3 spatial resolution from the 7.5 mm available in the PCOS readout to 200 μm.

The four cathode readout strips in each cell used to resolve the L/R ambiguity are preamplified at the chamber, and follow the same route as the cathode strips of WC1 and WC2, described earlier. In total there are 576 channels of FASTBUS ADCs associated with the cathode strips of WC3. Since these strips are vertical and are used for resolving the L/R ambiguity, no vertical information is available from WC3. The width of the ADC gate used to digitize the WC3 cathode signals is larger than that used for WC1 and WC3 to account for the longer drift time in WC3: a gate 500 ns wide is used for WC3 (and WC4).

The $\geq$150 ns drift time prevents this chamber from operating safely in the narrow angular regions where the incident pion beam passes through the chamber. Therefore, the incoming and outgoing beam regions in WC3 are deadened by turning off the anode voltage for the affected cells. A special high voltage patch panel was built which permits grouping of four WC3 cells either to ground or to high voltage. Typically one such group of four cells is deadened in the incoming beam region, and two groups are deadened in the outgoing region.

The construction of this chamber is similar to that of WC1 and WC2 in that two concentric 1 mm-thick rohacell cylinders separated by 7.5 mm are used to support the wire tension. In this case, however, the G10 support rings are drilled to accept crimp pins through which the anode and cathode wires are strung and crimped. The same technique used in WC1 and WC2 is employed to join the WC3 cylinders and provide a gas tight seal. The anode wires are 50 μm diameter gold-plated tungsten tensioned to 100 g. The cathode wires are 100 μm in diameter tensioned to 150 g. The anode and cathode wires are 90 mm in length. Each of the four vertical cathode readout strips in a given cell is 4 mm wide, and the field shaping cathode strips are 3 mm wide. The foils applied to the rohacell cylinders of WC3 are identical in thickness and composition to those of WC1 and WC2, except the outer surface of the inner WC3 cylinder consists of an etched ECN foil instead of plain aluminized mylar. Gold-plated spring clips were again used to achieve reliable electrical contact between the strips and the cylindrical circuit board to which the preamplifiers connect. As with the inner two chambers, additional 25 μm aluminized mylar foils ($\pm$9.8 mm from the anodes) are employed to provide a flushing volume and improved electrical isolation. The chamber is seated in an eccentric ring stand of design similar to that of the inner two chambers.

The high voltage requirements of WC3 are +2.250 kV on the anodes, $-$600 volts on the cathode wires, and $-$300 volts on the field-shaping cathode strips. The efficiency of the chamber at this voltage is typically 94%. The four cathode readout strips in each drift cell receive no high voltage. Both WC3 and WC4 use a drift gas

mixture of argon-ethane (50:50) with an additional 0.4% ethanol as a quenching gas. The flow rates are similar to the first two chambers (100 cm^3/minute), however the volumes are quite different: WC3 has a volume of 2 liters, and WC4 has a volume of 10 liters.

The relatively low and spatially-varying electric field produces a large Lorentz angle and hence electron trajectories are highly curved. Coordinate reconstruction from the drift time is complicated by the dependence on the track angle of incidence, the drift time, and magnetic field strength. The chamber is calibrated with an iterative technique which uses the actual data acquired in a given CHAOS experiment. A two-dimensional lookup table of drift time and track angle contains best estimated drift distances. A large number of tracks is analyzed and residuals are collected. The residuals are defined as the differences between the coordinates obtained from the WC3 lookup table, and those obtained from a least squares fit using coordinate information from all four wire chambers. These residuals, averaged for each TDC bin and each 2° track angle bin, are used to improve the look-up table used in the next iteration. This process is repeated until satisfactory convergence is achieved. At present, the same drift time to distance relation is used for all cells. Furthermore, the anodes are assumed to lie in a cylinder of radius 343.78 mm. The offsets and rotation of this cylinder in the spectrometer plane relative to the other chambers are also determined by a fitting procedure.

6. The Vector Chamber WC4

Although in principle the inner three chambers discussed above are sufficient to determine the momenta of charged particle tracks in CHAOS to a few percent, the design Monte Carlo calculations indicated a fourth chamber was necessary to bring the momentum resolution of the spectrometer to the 1% level. A fourth chamber was also deemed necessary to resolve potential track sorting ambiguities. The calculations indicated that the chamber should be situated at a radius near 650 mm (where the magnetic field of the spectrometer has fallen to 10 or 20% of its central value) and that the spatial resolution required was stringent enough that a drift chamber was necessary. On the other hand, since this chamber is positioned at the end of the charged particle track, multiple scattering was no longer of much concern and a completely different design could be used which incorporates several (cylindrical) anode planes within one chamber.

A trapezoidal cell geometry was chosen (see fig. 6), similar to that used in ref. [10] but incorporating several improvements over that design. Each of the 100 cells in WC4 is 3.6° wide and consists of 14 anodes staggered alternately $\pm$250 μm perpendicular to a radial line bisecting the cell. The anodes of WC4 therefore define 14 concentric cylindrical planes, or layers. The radius of the first layer is 612.50 mm and successive layers are separated by 5 mm. The drift times to the middle eight layers are digitized to provide the vector associated with the track passing through the cell. Layers 2 and 13 consist of resistive wires which are used to determine the vertical coordinate of the track at those anode radii by the method of charge division. Layers 1, 3, 12, and 14 consist of guard wires used to tailor the electric field in the cell. In this region of low spectrometer field, a straight line is used to approximate particle tracks over the 4 cm active depth of WC4.

Rather than use cathode wires to define the boundaries between adjacent cells, which dramatically increases the wire tension to be supported, cathode strips were used in a novel scheme which actually helps support the chamber instead. This scheme was implemented using C-shaped frames of 1.6 mm-thick G10. Rohacell sheets 2 mm thick were glued into the opening of the G10 C-frames. 25 μm-thick ECN foils with the cathode strip pattern photochemically etched on one side were glued to each face of the G10/rohacell assembly. While the glue was still wet, the

entire assembly was placed in a steel mold heated to 160° and compressed to a thickness of 1.6 mm in a 1 ton hydraulic press. The cathode strip pattern on each foil consists of nine 7.4 mm wide strips separated by 1.0 mm. Since the drift cells are trapezoidal, the cathode voltage is dropped 55 volts across each strip by means of a chain of 3.02 MΩ resistors in order to keep the electric field in the cell uniform and perpendicular to the row of anode wires. A larger resistance drops the voltage on the last (innermost) strip to ground. The circuit pattern for the resistor chain is etched on each side of the G10 frame and connected to the cathode strip pattern via gold-plated spring clips.

The top and bottom of the chamber consist of 8.5 mm-thick ultem plates which were drilled to an accuracy of 20 μm with the anode wire pattern. The holes were drilled 1.00 mm in diameter to accept crimp pins through which the anode wires were strung and crimped. An upper and lower ultem plate were held 231 mm apart by means of the G10 C-frames with the cathode strip patterns (ribs), as well as by a 250 μm-thick backwall of G10 glued to the outer edge of both ultem plates. This outer G10 window was copper laminated on the inside surface and nickel plated to provide an outer cathode plane common to all cells of the chamber. The spine of the G10 C-frames was glued to this outer window, and the chamber was further strengthened by gluing 1.6 mm thick G10 spines to the outer surface of the outer G10 window directly behind each C-frame spine, effectively continuing the C frame spine through the outer window another 15 mm. The C-frames were further attached to the ultem plates by means of grooves in the top plate into which they were glued, as well as slots in the bottom plate to which they were also glued. The resistor chain circuit pattern on each C-frame protrudes through this slot beneath the lower ultem plate. With the outer window and C-frames glued in place, the chamber was strung with the anode wires. The inner window was fabricated with 1 mm-thick rohacell containing a 12 μm-thick kapton foil on the outside and a 25 μm-thick aluminized mylar foil on the inside. The aluminized mylar formed the inner cathode surface common to all drift cells of the chamber.

Due to the large diameter of the chamber it was built in eight sections: four of these were 36° wide and four were 54° wide. All eight sections were mounted together on a common ring rigidly attached to the magnet.

The eight drift anodes in each cell consist of 20 μm diameter gold-plated tungsten tensioned to 50 g. The two resistive wires per cell are 20 μm diameter Stablohm 800 tensioned to 10 g. The resistance of these wires is approximately 1 kΩ over the 25 cm length of the wire. The guard wires are 150 μm and 75 μm gold plated tungsten. The operating bias of WC4 is −5.2 kV applied to the cathode strips, as well as −2.3 kV applied to the inner and outer cathode windows. It shares the same gas system as WC3.

The drift anode signals are preamplified at the chamber and followed a similar path as described for the anodes of the other chambers, through LeCroy 2735DC amplifier/discriminators to the 4290 TDC system. The resistive wires were treated differently from the cathodes of the other chambers, however. Short coaxial cables were used to bring the pulse from the bottom of the resistive anode wires to preamplifiers mounted on top of the chamber which also preamplify the signals from the top of the resistive wires. Two channels of the same quad Fujitsu MB43458PF preamplifier chip were used for a given resistive wire. The pulses were then delivered on 3 m-long alpha 9374 coaxial cables to cards located in crates situated on each of the four corner yokes of the magnet which consist simply of passive adapters for different connector types. The signals from these cards then follow the same route through the same type and length of delay cables as used for the chamber cathodes and are delivered to the FASTBUS ADC system. A 500 ns wide ADC gate is used.

Since the maximum drift time to the anodes of WC4 is ~450 ns, the cells illuminated by the incident beam were deadened in a procedure similar to that described for WC3. The cathode strips were grounded in groups of two so that three cells

at a time were deadened in this procedure. Typically one group of three cells was deadened where the beam enters the spectrometer, and two such groups where the beam exits.

The L/R ambiguity in WC4 is solved by making use of the ±250 μm staggering of the anode wires. The drift times to those anodes staggered towards a given track are generally shorter than to those staggered away from the track. This technique works well for resolving the L/R ambiguity, however the absence of cathodes between each anode leads to problems. The avalanches on the wires closest to a given track occur earlier and produce large induced pulses on the neighboring wires. The pulse observed on the wires staggered away from the track is then the sum of the avalanche on those wires plus the induced pulse from the neighboring wires. This problem was corrected to a large degree by means of a second order resistor cancellation network [10] implemented on the input of the preamplifier circuit boards of each cell.

The spatial resolution provided by the drift anodes of WC4 is easily measured by constructing the residuals of the wires, defined for anode wire i as

$$R_i = \frac{t_{i+1} - t_{i-1}}{2} - t_i, \qquad 2 \le i \le 7 \tag{1}$$

A typical residual histogram is shown in fig. 7. Two peaks separated by 1 mm (twice the stagger) appear, which are associated with whether the track passed to the left or right of the anode plane. The small difference in the width of each peak is a result of an imperfect cancellation network, as described above. The figure shows that the average spatial resolution for a single wire is 120 $\mu(\sigma)$. The vertical spatial resolution provided by the resistive anode wires is 2.3 mm (σ), better than 1% of the length of the wire.

The homogeneous electric field (~ 2 kV/cm, ≤ 100 V/cm variation) and the much lower magnetic field at the WC4 radius allow a straightforward drift time to distance relationship. We have parametrized the perpendicular distance from the anode wire plane to the track by:

$$d = v(TDC - t_0)[\cos(\theta_l) + \tan(\phi) \times \sin(\theta_l)] + \frac{5}{8} \times \tan^2(\phi)$$

where the drift velocity v and the Lorentz angle θ_l are adjustable parameters. ϕ is the track angle of incidence, and t_0 is the TDC offset. The first two terms are geometrical corrections to drift trajectories of angled tracks. The last term is a correction for the curved field lines near the anode wire [10]. Iterations on a large set of tracks are carried out to establish optimum values for v and θ_l for each setting of the magnetic field. v and θ_l are presumed common to all cells of WC4. The WC4 anode positions are assumed to be perfectly cylindrical. As with WC3, the center and rotation of the WC4 cylinder are optimized with respect to the other chambers.

7. The CHAOS Fast Trigger Counters and First Level Trigger

The readout systems for the wire chambers require gates and strobes. In particular, the 1696 analog signals digitized by the FASTBUS ADC system are delayed 210 ns, so an ADC gate must be issued within that time interval for those events deemed interesting. An appropriate condition on which to base this decision is the event multiplicity, which corresponds to the number of charged particle tracks produced in an interaction of the beam with the target falling within the detector acceptance.

The CHAOS fast trigger (CFT) counters were designed for this purpose, as well as to provide particle identification (π, e, p, d) of all detected tracks. The

counters are assembled in 20 adjacent blocks each 18° wide, situated just outside the WC4 radius in a contiguous cylindrical array concentric with the chambers. Each block consists of three elements. The innermost element (ΔE_1) is a 3 mm thick NE110 scintillation counter 178 mm (±7°) high. It is a cylindrical segment 18° wide (226 mm) with a radius at its inner surface of 720 mm. The ΔE_1 counters define the 1.54 steradian total geometric solid angle of the detector. Just behind these counters is a pair of adjacent 9° (115 mm)-wide NE110 scintillators 12 mm thick and 180 mm high denoted ΔE_2L and ΔE_2R. The third and outermost element of the detector is located just outside the ΔE_2 counters and consists of SF5 (radiation length 2.55 cm, n=1.70) used as a Čerenkov detector. 125 mm-thick blocks of SF5 are joined together to form a trapezoid with a frontal area of 237×223 mm^2 and rear dimensions of 275×253 mm^2. Three lucite light guides collect light from the rear of each SF5 block. Each ΔE_1 is viewed by a Hamamatsu R329-02 photomultiplier tube (PMT), as are the three lucite light guides in each SF5 block. The ΔE_2L and ΔE_2R counters are each viewed by an EMI 9815B PMT. All PMTs are shielded with iron and μmetal, and the lucite light guides for each counter place the PMTs well outside the spectrometer magnet where the fringe fields are within acceptable limits.

A gain monitoring system for the 120 PMTs comprising the CFT blocks is based on a xenon lamp which is flashed at regular intervals. The light from each flash is delivered to the light guides of each counter via optical fibers, and the light output is calibrated using a reference PMT and scintillator in contact with a ^{207}Bi source. This system is described in detail in ref. [11]. The PMT high voltage is supplied by a bank of eight Power Designs 1570 3 kV, 40 mA high voltage power supplies feeding a (PC) computer-controlled CAEN SY170 high voltage distribution system.

Only 18 of the 20 CFT blocks are in use at any given time. One block is removed where the beam enters the spectrometer, another is removed where the beam exits the spectrometer. Eight of the CFT blocks are situated just inside the four return yokes in the corners of the magnet. These blocks are fixed in place. The other 12 blocks are mounted on carts that can be rolled in and out of the spectrometer on bearings to facilitate block removal for beam entry and exit.

Ancillary counters include a four element scintillation counter hodoscope (S_1) consisting of 3.2 mm-thick horizontal strips 10 cm wide and each 7.5 cm high. This counter is situated just downstream of the last quadrupole magnet in the pion beamline. A second scintillation counter hodoscope (S_2) is situated just upstream of WC4 where the beam enters the spectrometer. It consists of four vertical strips 1.6 mm thick and 10 cm high. The middle two strips are each 8 mm wide and the outer two strips are 12 mm wide. A pair of veto counters (V) similar in size to the ΔE_2 counters but only 3.2 mm thick is situated where the beam exits the spectrometer in place of the CFT block that would otherwise occupy that position. Depending on the experiment, a first level trigger strobe is formed from the coincidence $S_1 \times V$, $S_2 \times V$, or $S_1 \times S_2 \times V$.

The output of each CFT PMT is delivered on coaxial cables to a bank of LeCroy 4413/200 high impedance-bridged input discriminators. The (bridged) analog output is delayed 120 ns with RG174/U coaxial cables and the pulse heights are digitized with LeCroy 4300B FERA ADCs. The ECL output of the discriminator is delayed and fanned out in LeCroy 4518 modules. One of the three 4518 outputs provided for each PMT signal is scaled in CAEN C257 CAMAC scalers. Another output is fed to programmable logic units (LeCroy 4508 PLU). The third 4518 output of the ΔE_1 and ΔE_2 scintillators is delivered to Phillips 7186H TDCs. The 4508 PLUs are programmed with the coincidence requirements for each CFT block desired in a given experiment. Usually this consists of a coincidence between ΔE_1(i) and the logical OR of ΔE_2L(i) or ΔE_2R(i) for CFT block i. If the requested coincidence pattern in

a given block is present when the first level trigger strobe is applied to the PLUs, an output for that block is fed to an input of a pair of LeCroy 4532 majority logic units (MALUs) which count the number of such coincidences among all CFT blocks. The MALUs may be programmed to provide an output when 1 or more such coincidences are present, or when ≥2 are present, and so on, thus establishing the desired event multiplicity. The MALU output is the first level trigger. It passes through a final coincidence to check whether the data acquisition computer is busy or not, and then is fanned out to provide all the gates and strobes required by the various electronic readout systems, as well as to start the second level trigger decision-making process. The propagation time through the first level trigger is only 100 ns, and it has been successfully tested at rates up to 35 MHz. The CHAOS CFT counters and first level trigger are explained in detail in ref. [12].

8. Second Level Trigger

Since high incident beam rates and large physical backgrounds are typical of the experiments planned with CHAOS, the rate of first level triggers can easily exceed the capability of the data acquisition computer. Restrictions on the events passed to the data acquisition computer beyond those established by the first level trigger are therefore required. This is accomplished by the CHAOS second level trigger (SLT), a programmable hardware trigger system based in CAMAC ECL modules which filters events passed by the first level trigger. The conditions which the SLT requires are developed in stages. The main stage requires the existence of a track defined by hits in WC1, WC2, and WC3, a track momentum within a specified range, a specific track polarity, an interaction vertex (actually a distance of closest approach of a track to the origin) within a specific range, and a specific range of incoming trajectories (used to reject muons arising from pion decay along the pion channel which contaminate the incident beam). Two optional, additional stages are also available. One is a p-θ stage which requires a specific correlation between track momentum and scattering angle. Another is useful for coincidence experiments, specifically $(\pi, 2\pi)$ reactions, and requires that two tracks pass the main stage and further that the sum of the momenta of these two tracks falls within a specified range.

The SLT bases its decisions on the wire numbers associated with hits in the inner three wire chambers delivered by the ECL output of the PCOS III electronics. All hits recorded by each of WC1, 2, and 3 for a given event are stored in LeCroy 2375 data stacks and all possible combinations of these hits are tried until a successful combination is found which satisfies the preprogrammed conditions. If no successful combination is found, or if there is not at least one hit in each of WC1, 2, and 3 to begin with, the SLT issues a fast clear to all the electronic readout systems and the event is rejected prior to ever being acknowledged by the data acquisition computer.

Use is made of the rotational symmetry of CHAOS to reduce the word size required to represent each hit combination.

All trial tracks are rotated such that the WC2 hit is at zero degrees, effectively eliminating WC2 from the subsequent calculations. The rotation is accomplished using LeCroy 2378 arithmetic logic units. The heart of the trigger, however, is in the extensive use of memory lookup units (MLUs) which are preprogrammed with the result of the trigger criteria for every possible input pattern. Several LeCroy 16 bit 2372s are employed as well as more powerful 21-bit MLUs designed and built at TRIUMF for the CHAOS SLT.

The time required for a decision from the SLT depends on the number of hits recorded by each of the three inner wire chambers, and on how soon a successful combination of hits is found. The typical time required for an event to be tested on all the conditions listed above is 2-4 μs. Typical event rate reduction factors provided

by the SLT are between 10 and 1000. The SLT is described in detail in ref. [13,14].

9. Acquisition System

The readout electronics for the various elements of the detector consist of ordinary CAMAC modules, FASTBUS, and special systems (PCOS III and the 4290 system). CHAOS was commissioned using a slow but well-understood data acquisition system based on CAMAC and running in a J11 Starburst microprocessor. After the detector was commissioned, the acquisition system was changed to a VME system based on a preliminary version of the CEBAF online data acquisition system CODA. All readout systems which deliver ECL output are funneled into LeCroy VME 1190 dual port memory modules which store all the zero-suppressed data from that readout system for a given event. VME 1190 modules receive data from the PCOS III, FERA, and FASTBUS systems. The FASTBUS ECL data are formed by implementing a LeCroy 1821/ECL 'personality' card on the auxiliary backplane of the FASTBUS crate behind the 1821 segment manager/interface. Unfortunately, no ECL output is provided with the 4290 system or with the Phillips TDCs. Those systems as well as miscellaneous other CAMAC modules are read out with a VME/CAMAC interface (CES CBD8210) residing in the VME crate. This interface is also used to initialize and program all the various readout systems as well as the first and second level triggers prior to the start of any given data acquisition period. There are approximately 4800 channels of information provided by the detector. The zero-suppression features of the various readout systems reduce the length of typical events to approximately 450 bytes per event, depending somewhat on the trigger settings.

The processor in the VME crate is a Motorola MVME 162-23 running VX-Works. This task is connected by ethernet to a DECstation 5000 model 240 running CODA. A data distributor (DD) task is also running on this DECstation which distributes the events delivered by CODA to a storage medium (disk or 8 mm tape) as well as to a DEC alpha 3400 on which the online analysis software runs. The latter connection is also via ethernet. The online analysis software consists of several hundred subroutines, mostly written in extended FORTRAN 77, and makes use of the Fermilab YBOS data organization scheme. All the above processors are isolated from the TRIUMF site ethernet traffic by means of an ethernet bridge.

Extensive modifications were made to the original CODA and DD packages to adapt them for use with the hardware configuration used in CHAOS as well as to fix bugs and implement new features. The resulting system requires about 6 μs per CAMAC access, an order of magnitude longer than the direct memory access of the VME memories. Roughly 2/3 of the data for each event are read from VME, and 1/3 from CAMAC. An additional 25 μs are required to serve the hardware interrupt delivered to the front panel of the CES8210 in the VME crate. Rates associated with a typical run are on the order of 200 events per second (90 kbytes per second) for data recorded to tape, with a 75% live time associated with the data acquisition system. Approximately 20% of these data are fully reconstructed online with the alpha.

10. Auxiliary Systems

A number of auxiliary systems are used in conjunction with the spectrometer. Only a few of these are mentioned here. One such system is the CHAOS test pulse (CTP) system. All the preamplifiers of the wire chambers contain a test pulse input which is capacitatively coupled to the preamplifier inputs. The WC1 and WC2 anodes are instrumented with 16-channel preamplifier boards, and everything else in the detector with 8-channel preamplifier boards. A system of shift registers allows

any desired pattern of preamplifier boards to be fired at a rate given by a NIM pulser. The pattern is chosen with a program running on a PC in the windows environment. The CTP system is useful in identifying and locating dead channels in the detector which can occur anyplace downstream of the actual wire chambers, but typically arise from failures of the preamplifiers themselves. With almost 4800 channels to monitor, the CTP has proven to be an indispensible tool.

Another monitoring system (MONITOR) runs on a PC under the windows environment which monitors a variety of experimental parameters, including the beamline magnet values, CAMAC and VME scalar values and ratios, wire chamber voltages and currents as well as other voltages and currents such as those associated with the CFT PMTs, and any calculated quantities from any of the processors involved with the detector which can be reached via ethernet. The MONITOR program checks the values of each parameter it is programmed to monitor to see if it is within supplied limits. Graphs of the values of requested parameters are displayed in separate windows as a function of time. If a parameter goes out of range, an alarm sounds and the offending channel as well as the specific alarm condition is announced over a speaker in the counting room.

Standard Bertan high voltage wire chamber power supplies were modified such that the high voltage for each wire chamber could be controlled by a HV control program, again running on a PC under windows.

Many interesting software tools were developed to facilitate operation of the spectrometer. One is the ECL program which provides a simple-to-use interface between the experimenter and each of the various programmable ECL modules contained in the first and second level trigger. This tool is useful for the initialization of all these modules as well as for debugging. Another such tool was developed for FASTBUS gymnastics. Further tools were developed to calibrate the wire chambers, providing spatial and rotational offsets for all four chambers as well as time to distance relations for the drift chambers.

11. Detector Performance

The results presented here were obtained from data acquired in connection with $(\pi, 2\pi)$ experiments initially performed with CHAOS in 1994. As such, they represent performance typical for the detector.

To summarize the detector elements described in the preceding sections and to introduce the concepts discussed in this section, a typical event recorded by the spectrometer for the $\pi^+ n \longrightarrow \pi^+\pi^- p$ reaction is shown in fig. 8. The incident beam was 400 MeV/c π^+ and a liquid deuterium target was in place at the center of the spectrometer, which was set to a field of 0.5 T. The figure shows the incoming beam trajectory, which is reconstructed using the hits in WC1 and WC2 in conjunction with the known incident beam momentum. The three reaction products are also reconstructed and labeled in the drawing with a track number (1,2,3). The momentum reconstruction uses the hits in all four wire chambers for each track, as well as the result of particle identification provided by the CFT blocks. The missing energy reconstructed for this event is less than 5 MeV. The interaction vertex and scattering angle of each outgoing track are obtained by extrapolating each trajectory inside the WC1 radius and intersecting it with the incident beam trajectory.

The analysis software which reconstructs the observables from the raw data provided by the detector makes use of the Fermilab YBOS format. Initially, the raw data are converted to spatial coordinates for each of the wire chambers. A preliminary L/R decision is made for each hit recorded by WC3. The hits recorded by WC4 are sorted into independent tracks (which may cross up to three adjacent WC4 cells) and a preliminary L/R decision is made for those tracks, which provides a starting

vector for each WC4 track. This vector is used to start the overall track sorting procedure, which links the appropriate hits in each of the three inner chambers with each track found in WC4. Each track is allowed to have up to one missing chamber. The incoming beam track defined by the appropriate hits in WC1 and WC2 is also identified at this stage, and its trajectory is reconstructed analytically using the known incoming beam momentum.

Once the hits have been sorted into tracks, the momentum and trajectory of each track are obtained using a quintic spline technique derived from that described by Wind [15]. With the trajectory of each track determined in the plane perpendicular to the spectrometer field, the vertical component of the trajectory of each track can also be determined by making use of the cathode information provided by WC1 and WC2. At this point the incoming beam trajectory can be intersected with the outgoing particle trajectory to obtain the scattering angle and interaction vertex. If more than one outgoing track is present, the interaction vertex may be obtained by intersecting two outgoing trajectories as well.

Particle identification is accomplished by combining the pulse height information provided by the CFT counters with the track momentum. A scatterplot of the energy loss of particles traversing ΔE_1 versus the momentum of those particles is shown in fig. 9. Events from all 18 ΔE_1 counters are overlaid in this plot. The fact that the resulting particle bands are still clearly distinguished is due to the careful matching of gains from all the CFT counters, which is accomplished beforehand using two body reactions such as pion absorption and πp scattering, and monitored using the Xenon flasher system described earlier. Protons are easily separated from other particles as shown in fig. 9; the π–p discrimination efficiency is greater than 99%. Pions and electrons (or positrons) are well separated from each other for momenta less than about 150 MeV/c. For momenta greater than this, the pulse height deposited in the Čerenkov counters must be examined to distinguish pions from electrons. A scatterplot of the Čerenkov pulse height (all counters overlaid) versus momentum is also shown in fig. 9. The group of events with small pulse heights is the pions, which produce little Čerenkov light in the top lead glass relative to the electrons. The electrons and positrons can be identified as the bands extending to large pulse heights in fig. 9. Combining the information provided by the ΔE_1, ΔE_2, and Čerenkov counters provides an overall π–e discrimination efficiency in excess of 98% for particles in the momentum range 0–250 MeV/c. Above this momentum the π–e discrimination efficiency drops to 93%.

Three categories of muons must be considered. The CFT counters do not provide $\pi - \mu$ discrimination. Those muons which arise from pion decay at the pion production target have the same momentum and trajectory as the pions delivered by the beamline. These muons pass through the deadened regions of the drift chambers and are vetoed along with the noninteracting pions by the veto counters at the exit of the spectrometer. Muons which arise from pion decay somewhere along the beamline upstream of the CHAOS target are eliminated by second level trigger requirements. These requirements constrain the trajectory of the incoming beam to pass through narrow windows in WC1 and WC2 as well as through a narrow cylinder at the origin of the spectrometer. This effectively constrains the momentum and trajectory of incoming particles such that most of these muons are eliminated. The third class of muons consists of those which arise from pion decay after the CHAOS target, and are the most difficult to identify. If the decay occurs inside WC1 it is more difficult to distinguish these events from scattered pions. They may still be eliminated if a coincidence requirement has been established, or if the reconstructed vertex falls outside the target volume. For large enough spectrometer fields, almost all muons which are produced from the decay of noninteracting pions are deflected onto one side of the scattering angle distribution, independent of the initial direction of the decay

muon. Muons which are produced outside WC1 can also be identified by comparing the momentum and trajectory determined by the inner three wire chambers with that determined from the outer three wire chambers. A mismatch is a good indicator of decay events.

The scattering angle and interaction vertex for each track can be computed once the momentum of each track has been established. Trajectories for the incoming beam track and each outgoing track are recomputed using the momentum and the equations of motion for a charged particle in a magnetic field. The magnetic field at each step is taken from the measured field map. The outgoing trajectory is followed from WC1 in to the target in small steps until the intersection with the incoming beam trajectory is found which lies closest to the origin. For those cases where no intersection is found due to the finite spatial resolution of the chambers, the distance of closest approach is taken as the interaction vertex. The scattering angle is taken as the angle between the tangents to the trajectories at the interaction vertex. The vertical coordinate of the interaction vertex is the intercept of the straight line fit to the z-coordinate versus the distance in the horizontal plane from the interaction vertex to the hits in each chamber delivering that z-coordinate. The vertical vertex resolution is limited by the WC1 cathode inefficiency resulting from the use of too low an initial operating voltage for that chamber. At present, this resolution is 2.2 mm but should improve as higher voltages are applied to WC1. A measure of the spatial resolution associated with horizontal vertex reconstruction is obtained by comparing the vertices obtained for outgoing pions and coincident protons resulting from πp elastic scattering. Using π^+p data acquired with a liquid hydrogen target for 280 MeV incident pions and a 0.5 T spectrometer field, the vertex resolution for a single track varies between 0.3 mm and 1.5 mm, depending on the scattering angle. This variation is a consequence of the difficulty of intersecting tracks which are nearly parallel or antiparallel (near 0° and 180° scattering angle) relative to those which are nearly perpendicular (near 90° and 270°). The scattering angle resolution is less than 0.5°. A typical scatterplot of the horizontal vertex reconstructed from πp elastic scattering events under the conditions listed above is shown in fig. 10. The 5 cm diameter LH_2 target is illuminated by the incident beam whose profile is less than that of the target. The good vertex resolution achieved in CHAOS is reflected by the sharp edges of the target vertex where the beam intersects the target.

Many of the unique and powerful features of the spectrometer are illustrated in figures of kinematic correlations. One such illustration is provided in fig. 11, which shows the angular correlation of events detected in the spectrometer for liquid deuterium and liquid hydrogen targets acquired under otherwise identical conditions (220 MeV incident π^+ with a spectrometer field setting of 0.5 T, and a coincidence trigger). The data contained in these plots were acquired in only a few minutes of acquisition time with each target. In each case two tracks were searched for, starting at 0° and searching out to 360° . The angle of the first track found is plotted on the horizontal axis, the angle of the second track found on the vertical axis. For the LD_2 target, events from the $\pi^+ d \longrightarrow pp$ reaction appear as a sharply defined band. The other bands are associated with πp quasi-elastic scattering in which either the pion or the proton is the first track found. These events are smeared out by the Fermi momentum of protons in the deuteron. This is most evident by comparing this with the LH_2 target scatterplot, in which the absorption events are absent as is the Fermi momentum. These free πp elastic scattering events appear as a very sharp band. Both targets illustrate the capability of the spectrometer to acquire coincidence data over an extremely broad angular range. The only angular regions missing are those near 0° and 180° where the combined effects of the deadened drift chamber regions and missing CFT blocks (where the beam enters and exits the spectrometer) are manifest.

A further illustration of the spectrometer's performance is provided by compar-

ing a histogram of the measured pion scattering angle distribution with the predicted differential cross sections from a phase shift analysis for π^+p elastic scattering (SAID FA93 solution). A preliminary comparison is shown in fig. 12 for 280 MeV incident π^+ on a LH_2 target. A spectrometer field setting of 0.548 T was employed for these data and a singles trigger (first level trigger requires one track, no second level trigger) was used. Although only a single track was required in the trigger, events for which the recoil proton was also detected can be analyzed separately and compared to the results obtained when only pions are analyzed. Such a comparison is made in fig. 12. All the data in this figure were acquired simultaneously in about twenty minutes of acquisition time.

The values used for the absolute normalization of the data shown in fig. 12 are: effective areal target density of 2.07×10^{23} protons per cm^2 ($\rho = 74$ mg/cm^3), nominal solid angle of 21.3 msr per 5° angular bin, overall wire chamber efficiencies of 96% (WC1), 92% (WC2), 84% (WC3), and 100% (WC4), reconstruction efficiency 100%, and acquisition live time 57% . The target density reflects the folding of the measured incident beam profile on the cylindrical target. Angle (momentum)-dependent corrections to the purely geometrical solid angle of 5° by 14° were made by means of a Monte Carlo calculation which took into account the vertical focusing provided by the fringe field of the spectrometer. The wire chamber efficiencies (for pions) were measured using events which contained a (recoil) proton track. For such events the trajectory of the corresponding pion was predicted from the measured angle and momentum of the proton. The efficiency of a given wire chamber for pions is then obtained simply by observing whether the chamber contained a hit for the pion in the expected location. Muon tracks were eliminated by further requiring that the WC4 track be present where expected, which is possible due to the eight-fold anode multiplicity per WC4 cell and resulting 100% efficiency of that chamber. The reconstruction efficiency and wire chamber efficiencies for protons can be obtained following a similar procedure. More accurate values for the spectrometer solid angle and pion survival fraction can be obtained by means of careful Monte Carlo calculations.

An interesting feature of the spectrometer is the fact that data are acquired at both $\pm\theta$. Since by virtue of parity conservation $d\sigma/d\Omega(+\theta) = d\sigma/d\Omega(-\theta)$, a built in systematic check of the spectrometer's performance is obtained from such a comparison. Holes in the scattering angle distribution are from the beam entry and exit regions. Although there is little one can do to affect the hole near 0° where the beam exits the spectrometer, the entry hole in the scattering angle distribution (near 180° in fig. 12) can be shifted to different locations depending on the spectrometer field setting (and veto counter configuration). As fig. 12 shows, the shape and absolute normalization of the measured angular distribution show good agreement with the predicted cross sections over the full range of scattering angles covered by the spectrometer, for both singles and coincidence data.

The momentum resolution of the spectrometer has been measured with a variety of techniques. With the momentum spread of the incident beam limited to 0.25% and the spectrometer field set to 1 T, the distribution of reconstructed momenta of 225 MeV/c pions has a width of 1.0% (σ). Although there is no upper limit to the momentum of particles which are detected in the spectrometer, clearly the momentum resolution deteriorates above some point for a fixed spectrometer field. Likewise, for lower momentum particles the effects of multiple scattering and energy straggling in the target and detector combine to worsen the momentum resolution. On the other hand, higher spectrometer fields for a fixed momentum generally improve the momentum resolution. As a result it is difficult to provide a fixed number for the spectrometer momentum resolution, however 1% is typical for routine conditions.

It is interesting to use the known level structure of ^{12}C as a realistic ruler

for measuring the CHAOS momentum resolution with a more favorable p/B ratio. Pion scattering on a 2.6 mm thick graphite target was studied using 139 MeV π^- and a 1.4 T spectrometer field. Elastic scattering was observed as well as inelastic scattering to the 4.44 MeV first excited state and the state at 9.6 MeV. The angular distributions of the differential cross sections to these three states, obtained between 40° and 160°, compare favorably to the published 150 MeV data of Binon, et al. [16]. The momentum resolution measured in this exercise was 0.87% (σ).

Acknowledgements

We gratefully acknowledge the assistance provided by the technical and support staff of TRIUMF, especially the TRIUMF detector group and the TRIUMF scintillator shop. We thank C. Becciani for his help in the construction of the CFT light guides, R. Openshaw and M. Goyette for help in the construction of the chamber gas system, S. Ritt, I. Bertram and S. McDonald for help in the development of the detector simulation package, I. Yhap, S. Sabaratnam and summer students J. Mondia, B. Jackson, B. Wilson, and D. Thiessen for help in constructing various subsystems for the detector. The financial assistance which made this project possible was provided by the Natural Sciences and Engineering Research Council (NSERC) of Canada as well as by the Instituto Nazionale di Fisica Nucleare (INFN), Italy. One of us (R.A.R.) acknowledges financial support received by the US DOE, another (E.F.G.) from the CSUS foundation, and one of us (H.M.S.) from the VW-Stiftung.

References

[1] A.A. Bolokhov, V.V. Vereshchagin, and S.G. Sherman, Nucl. Phys. **A530** (1991) 660 .

[2] J. Gasser and H. Leutwyler, Phys. Rep. **87C** (1982) 77 .

[3] J. Gasser, H. Leutwyler, and M.E. Sainio, Phys. Lett. **B253** (1991) 252.

[4] J. Gasser and H. Leutwyler, Phys. Lett. **125B** (1983) 321.

[5] G.R. Smith, TRIUMF Design Note TRI-DN-90-5, February, 1990.

[6] M. Kermani, MSc. thesis, Univ. of British Columbia (1993), unpublished.

[7] R. Openshaw, R.S. Henderson, W. Faszer, and M. Salomon, Nucl. Instrum. Methods **A307** (1991) 298.

[8] P.A. Amaudruz, et al., to be submitted to Nucl. Instrum. Methods (1994).

[9] G.J. Hofman, J.T. Brack, P.A. Amaudruz, and G.R. Smith, Nucl. Instrum. Methods **A325** (1993) 384.

[10] R.S. Henderson, et al., IEEE Trans. on Nuclear Science **37** (1990) 1116.

[11] F. Bonutti, P. Camerini, N. Grion, R. Rui, and P. Amaudruz, Nucl. Instrum. Methods **A337** (1993) 165.

[12] F. Bonutti, S. Buttazzoni, P. Camerini, N. Grion, and R. Rui, Nucl. Instrum. Methods **A350** (1994) 136.

[13] K. Raywood, P.A. Amaudruz, S. McFarland, M.E. Sevior and G.R. Smith, submitted to Nucl. Instrum. Methods (1994).

[14] S. McFarland, MSc. thesis, Univ. of British Columbia (1993), unpublished.

[15] H. Wind, Nucl. Instrum. Methods **115** (1974) 431,
Nucl. Instrum. Methods **153** (1978) 195,
H. Corporal, Nucl. Instrum. Methods **158** (1979) 127.

[16] F. Binon, et al., Nucl. Phys. **B17** (1970) 169.

Figures

1. A sketch of CHAOS. One of the four vertical iron corner return yokes and sections of detectors have been removed from this figure for clarity. The magnet hides most of the detector elements, which are located between the poles, from view.
2. Details of the central region of the CHAOS detector are presented. The detector array is actually completely cylindrical; in this figure parts of each detector component are cut away for clarity. The individual components are discussed in the text.
3. The radial field profile of the CHAOS magnet. The locations of the four wire chambers are also indicated by short vertical lines.
4. This side view shows a section of all detector elements to illustrate the geometry and construction of the wire chambers. Units are in mm.
5. The WC3 cell geometry. The cathode strip thickness and wire diameters have been exaggerated for clarity. The strips labelled H.V. are biased with -300 volts, the cathode wires with -600 volts, and the anodes with $+2250$ volts.
6. The cell geometry of WC4 is shown. The two dashed lines represent particle tracks through the cell. The features are described in the text. d and v refer to the drift time and distance. The inverse drift velocity 1/v is $\sim$20 ns/mm. θ_l refers to the Lorentz angle, typically 5° .
7. A histogram of the residuals calculated for a triplet of wires in a cell of WC4. The smooth lines are from a fit employing Gaussian lineshapes.
8. A typical event recorded by the spectrometer is shown. The axes are in mm. Struck anodes are indicated by a cross, as are the CFT blocks which contained signals for this event. The innermost two circles correspond to the 720 anodes per chamber of WC1 and WC2. The dotted circle represents the 144 anodes of WC3. The 100 radial line segments near an average radius of 640 mm correspond to the 100 cells of WC4, each of which has 8 drift anodes. Outside WC4 are the 18 CFT blocks, each 18° wide and comprised of a 3 mm scintillator (ΔE_1), followed by a 13 mm scintillator (ΔE_2), followed by a 120 mm lead glass Čerenkov detector. One CFT block is removed on the left of the figure to let the incident beam into the spectrometer, and another is removed on the right to permit the beam to exit. The drift chambers (WC3 and WC4) are deadened in these regions as well. Not shown in the figure are the 360 cathode strips per chamber in WC1 and WC2, 576 cathode strips in WC3, 200 resistive wires in WC4, and in-beam scintillation counters at the entrance and exit of the spectrometer.
9. A scatterplot of the momentum versus the pulse height in the ΔE_1 scintillation counter (a), ΔE_2 scintillation counter (b), or lead-glass Čerenkov counter (c) is shown to indicate the methods used to mass identify pions, protons, and electrons/positrons.

10. A scatterplot of the horizontal vertex coordinates for tracks identified as pions. The upper figure was acquired with an empty cryogenic target. The cryostat windows are clearly defined. The lower figure was acquired under the same conditions with liquid hydrogen in the target.
11. Scatterplots of the angles associated with coincident tracks detected in the spectrometer for a liquid deuterium target (upper figure) and a liquid hydrogen target (lower figure) under otherwise identical conditions.
12. The measured differential cross section as a function of scattering angle is shown for π^+p scattering data acquired at 280 MeV. The solid line is the prediction of the phase shift solution FA93. The upper figure contains those events for which only the pion tracks were analyzed. The lower figure is constructed from the same data, but contains only those events for which both pion and recoil proton tracks were present.

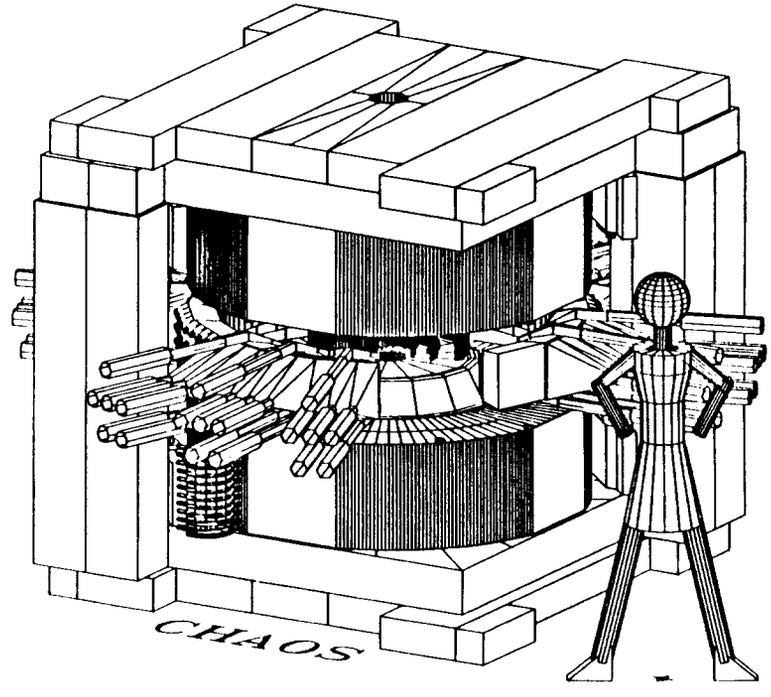

Fig. 1

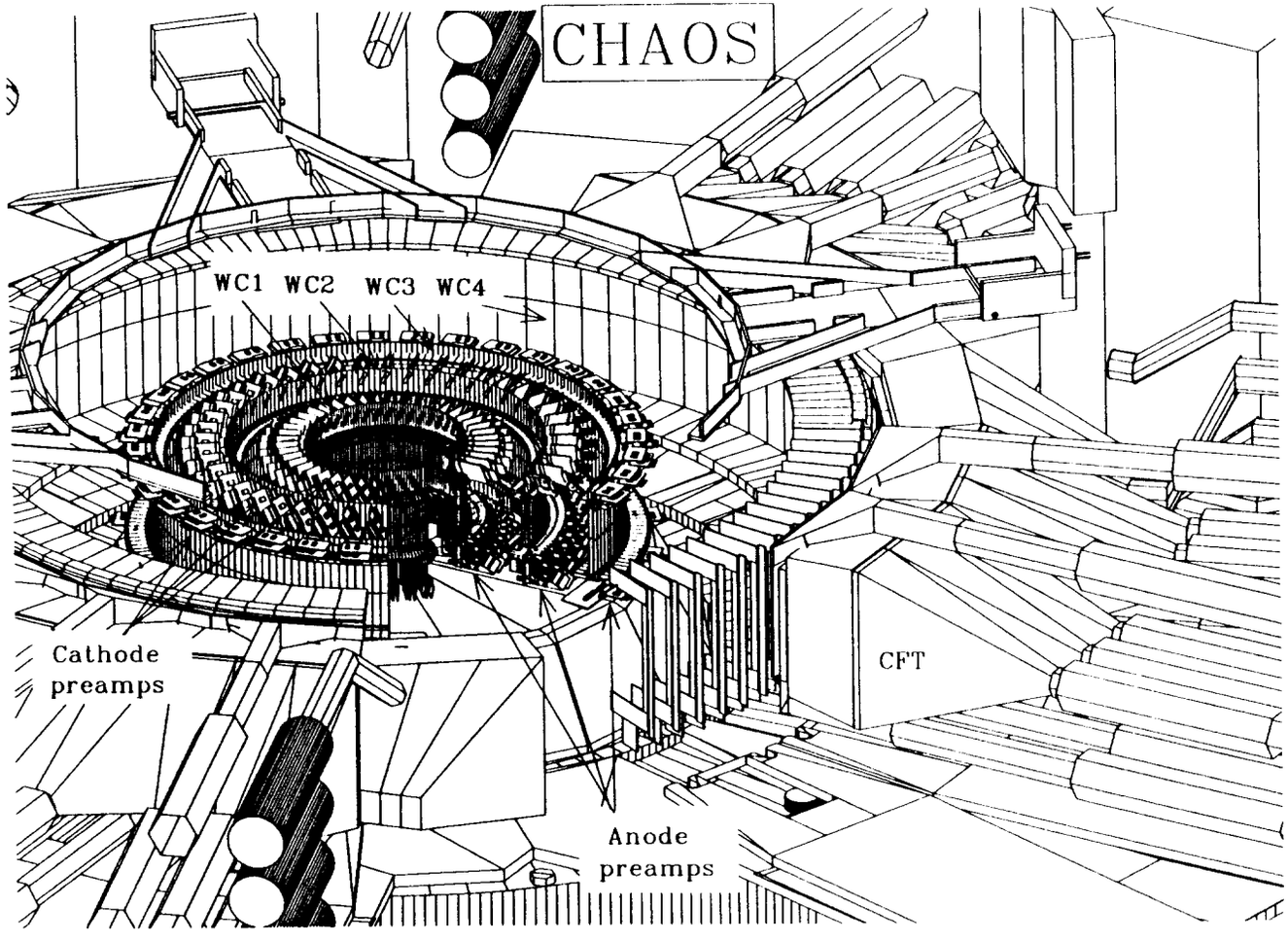
CHAOS
WC1 WC2 WC3 WC4
Cathode
preamps
CFT
Anode
preamps

Fig. 2

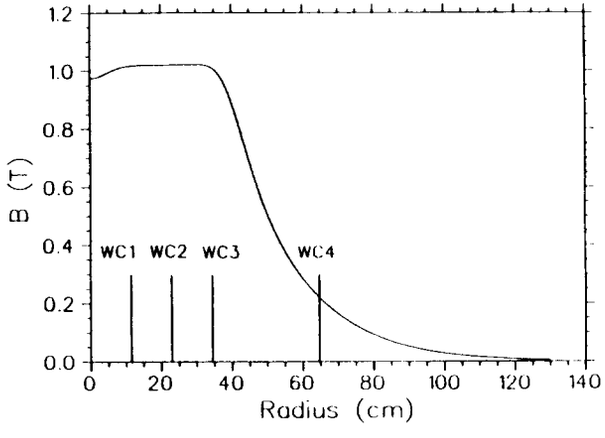
1.2
1.0
0.8
0.6
0.4
0.2
0.0
B (T)
WC1 WC2 WC3
WC4
0
20
40
60
80
100
120
140
Radius (cm)

Fig. 3

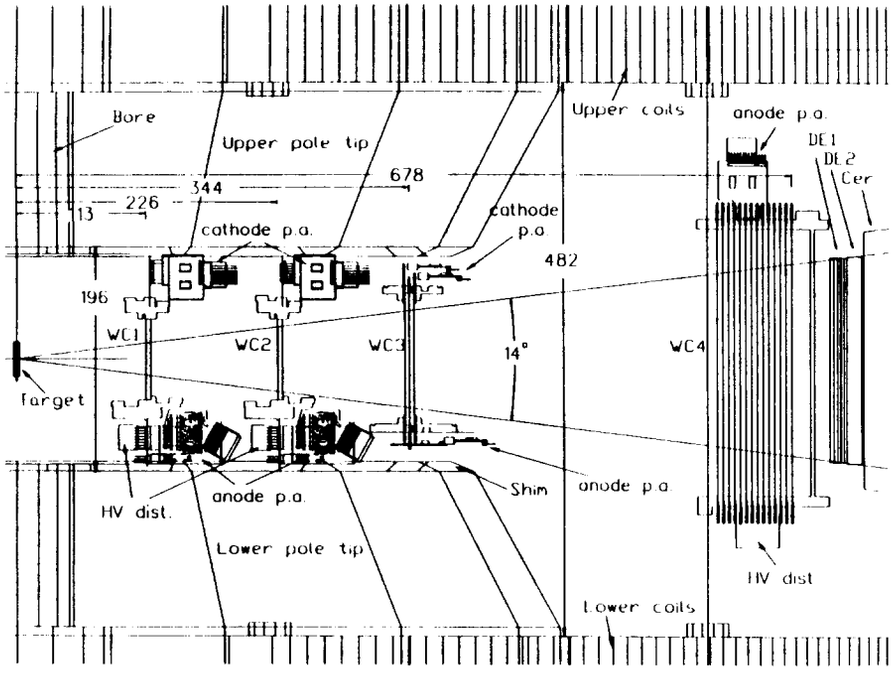

Fig. 4

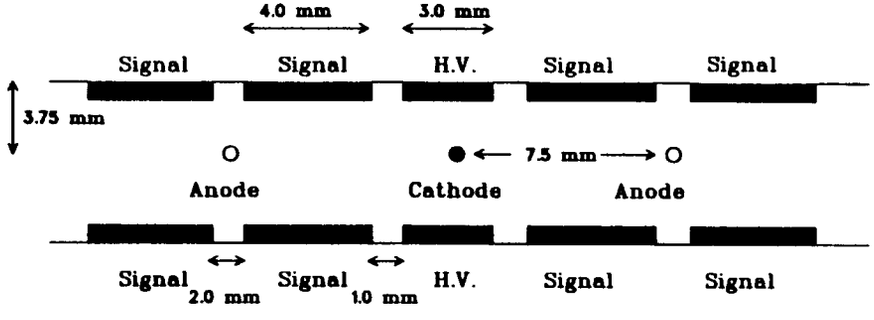

Fig. 5

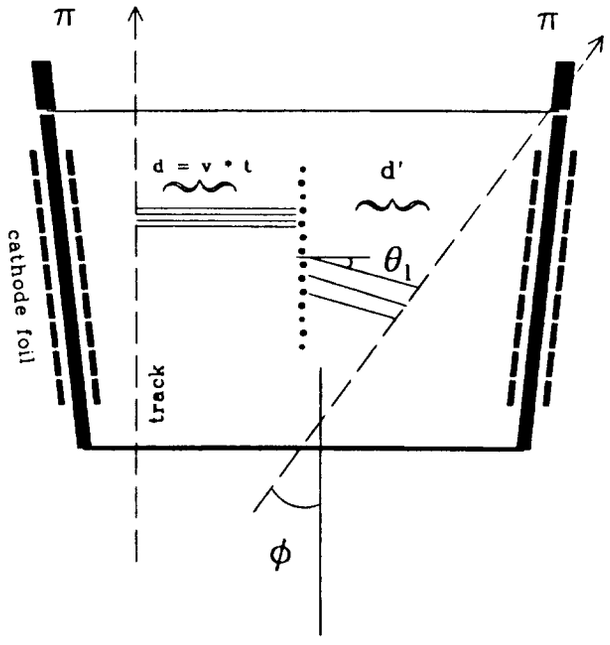

Fig. 6

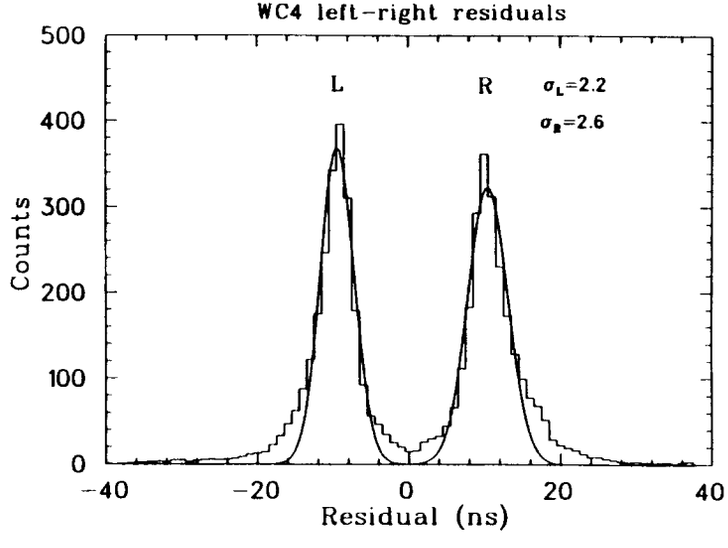

Fig. 7

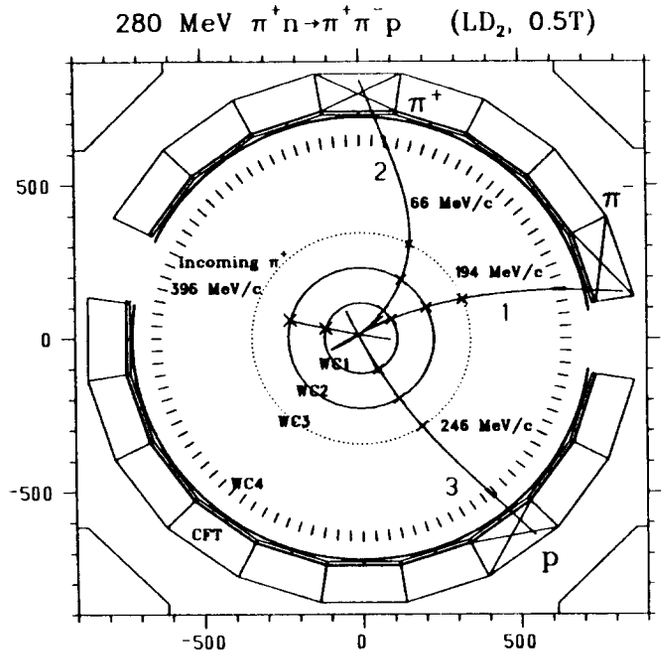

Fig. 8

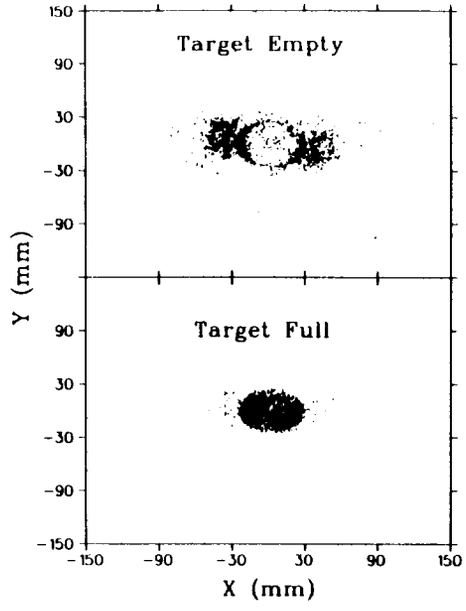

Fig. 10

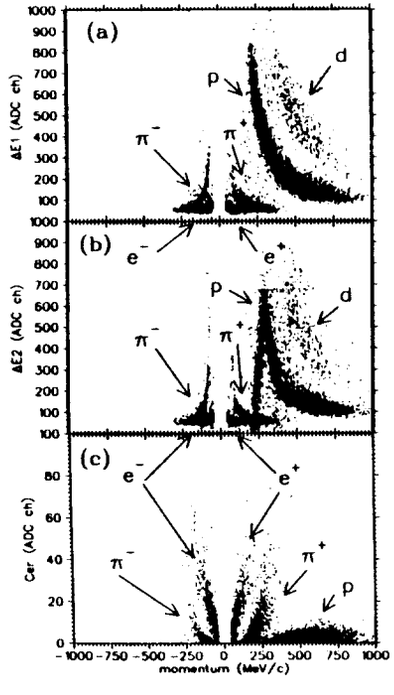

Fig. 9

Angular Correlations

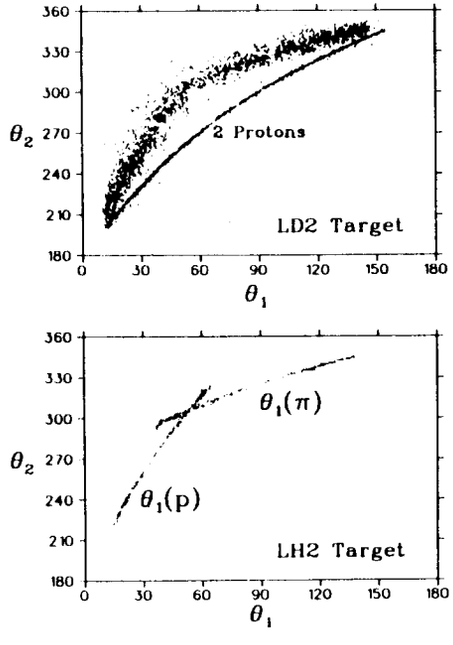

Fig. 11

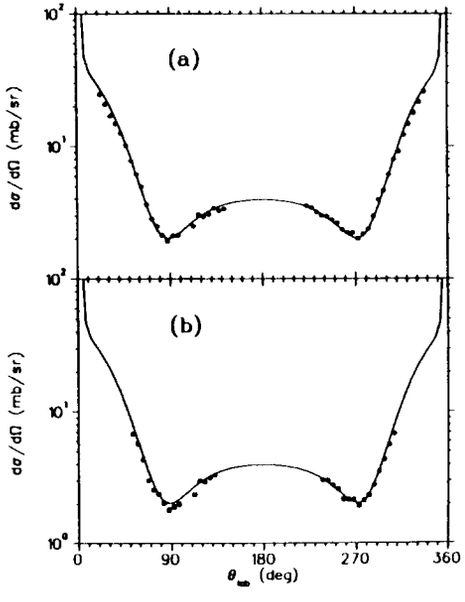

Fig. 12